Sustainable Chemistry for Climate Action 6 (2025) 100058

Contents lists available at ScienceDirect

Sustainable Chemistry for Climate Action

journal homepage: www.elsevier.com/locate/scca

Assessing sustainable latent heat energy storage of RT 35 phase change material in double pipe heat exchangers: A study on concentric and hairpin designs

Pallavi Kumari, Vinamr Saksena, Rishabh Jha, Debasree Ghosh *

Department of Chemical Engineering, Birla Institute of Technology, Mesra, Ranchi, India

ARTICLE INFO

Keywords:
Concentric double-pipe heat exchanger
Enthalpy-porosity model
Hairpin double-pipe heat exchanger
Latent heat thermal energy storage
Melting/solidification

ABSTRACT

To reduce the reliance on conventional fuels and mitigate environmental degradation, phase change materials (PCMs) offer a promising alternative. This study compares the performance of melting and solidification processes in hairpin and concentric heat exchangers (HEXs), with the goal of designing effective latent heat energy storage systems for both domestic and industrial applications. The research highlights that the time required for melting and solidification depends on several factors, including the thermal diffusivity and viscosity of the PCM. Although the energy contained in both concentric and hairpin heat exchangers is equal due to the same quantity of PCM used, the time required for energy storage is shorter in the hairpin heat exchanger (HHEX) (146 min) compared to the concentric heat exchanger (CHEX) (207 min). Additionally, the study underscores the significance of selecting the appropriate PCM, noting that PCMs with higher latent heat values has more energy storage capacity. However, the efficiency of energy storage also based on the variation in temperature between the high-temperature fluid (HTF) and the starting temperature of the PCM. The study finds that the energy storage capacity of the hairpin heat exchanger (HHEX) is 1.8 times greater than that of the concentric heat exchanger (CHEX) when using RT 35 as the PCM.

1. Introduction

During the last four decades, latent heat thermal energy storage (LHTES) has become necessary topic where researchers are still working to find the best energy storage techniques for storing renewable source of energy [1]. The advancement of technology and the improvement of living standards have greatly increased energy demand. The excessive use of non-renewable energy sources, particularly fossil fuels like coal, oil, and natural gas, is depleting these finite resources faster than they can be naturally replenished. The burning of fossil fuels releases greenhouse gases, primarily carbon dioxide (CO_2), into the atmosphere. As a result, the greenhouse effect has gotten stronger, causing climate change and global warming. [2,3]. According to a report, a significant portion of energy consumption in residential and commercial buildings goes towards space heating and cooling, with figures reaching up to 61 % and 40 %, respectively [4]. A comprehensive study by Isaac and Van Vuuren [5] predicts substantial changes: a 34 % reduction in residential heating demand due to climate change, while cooling demand is expected to surge by 72 %. To address these pressing concerns, countries are actively seeking clean and renewable energy sources to reduce reliance on fossil fuels. When compared to storing the same quantity of thermal energy through sensible thermal energy storage materials like concrete and water, LHTES offers an amazing advantage by possibly saving up to 90 % in mass and area [6]. These thermal energy storage systems are crucial for enabling the widespread adoption of renewable energy sources by addressing the issue of energy intermittency. Among the various thermal storage technologies, PCMs hold immense promise for thermal storage applications [7,8]. Extensive research in LHTES has been conducted, often involving theoretical and numerical investigations. This research aims to enhance the efficiency and feasibility of LHTES systems, making them more viable for large-scale applications. Integrating PCMs into these systems can optimize energy storage and release processes, contributing to a more stable and reliable energy supply from renewable sources. Furthermore, advancements in material science are continuously improving the thermal properties and cost-effectiveness of PCMs, boosting their potential for widespread use. In conclusion, while the increased energy demand driven by technological advancements and improved living standards poses significant challenges, innovative solutions like LHTES and PCMs offer promising

* Corresponding author.
E-mail address: dghosh@bitmesra.ac.in (D. Ghosh).

https://doi.org/10.1016/j.scca.2025.100058
Received 13 August 2024; Received in revised form 9 January 2025; Accepted 20 February 2025
Available online 21 February 2025
2772-8269/© 2025 The Authors. Published by Elsevier B.V. This is an open access article under the CC BY-NC license (http://creativecommons.org/licenses/by-nc/4.0/).

Symbols

PCM	Phase change material
HEX	Heat exchanger
LHTES	Latent heat thermal energy storage
HTF	High-temperature fluid
LTF	Low-temperature fluid
CHEX	Concentric heat exchanger
HHEX	Hairpin heat exchanger
C_{mushy}	Mushy zone constant
H	Enthalpy (kJ/kg)
β	Thermal expansion coefficient (1/K)
ρ	Density (kg/m3)
γ	Liquid fraction
v	Velocity component in y direction (m/s)
T_s	Solidus temperature (K)
T_l	Liquids temperature(K)
T_{ref}	Reference temperature (K)
T	Temperature (K)
$T_{initial}$	Initial boundary condition of heat transfer fluid
t_m	Melting time
t_s	Solidification time
ΔT_{Dr}	Temperature difference between HTF and initial temperature of PCM
S	Momentum source ($kg/m^2\ s^2$)
k	Thermal conductivity (W/m K)
L	Latent heat of solid/liquid phase change (kJ/kg)
g	Gravitational force (m/s^2)
St	Stefan number

pathways to a more sustainable energy future. By continuing to invest in and develop these technologies, it is possible to mitigate the adverse effects of fossil fuel dependency and pave the way for a cleaner, more resilient energy system. Hosseini et al. [9] performed experimental and numerical research on a shell and tube heat exchangers using RT 50 paraffin wax. They studied heat transfer specification and thermal behavior during melting and solidification process [10]. Esapour et al. studied the melting process of multi-tube heat exchanger (HEX) using RT35 as PCM. The results showed that the melting time is reduced by 29 % by increasing the number of tubes on the shell side [11]. Ismail et al. experimentally studied the solidification of PCM and the result showed that solidification time decreases by lowering the fluid inlet temperature [12]. Due to low thermal conductivity of PCM, the melting/solidification is prolonged and shows limitations to the energy storage device. Talebizadehsardari et al. numerically studied charging and discharging of a plate type HEX with modified zigzag configuration using RT 35 as PCM. The results showed the energy storage rate of system having 60° zigzag angle increases by 32.6 % when system having angle of 30° [13]. Said et al. numerically studied the melting performance of shell and tube HEX and to find out efficiency using RT 35 and RT 35HC as paraffin wax. The results concluded that using RT 35 has reduced the charging time up to 44 % and heat storage rate increases up to 3.2 % as compared to RT 35 HC due to lower heat storage capacity of RT 35 [14]. Fadaei et al. used enthalpy porosity model to thermophysical behavior of non-Newtonians PCMs, RT35 in shell and tube HEXs. The acquired findings showed that the non-Newtonian fluid of Carreau circulates at a quicker rate than the non-Newtonian fluid of Carreau-Yasuda and the Newtonian fluid by roughly 38 % [15].To solve this problem, various literature survey has been done using multiple tube in HEXs [16], external fins in multi-tube HEX [17], microencapsulation of PCM [18] vertical shell and tube HEXs [19]. Further, the authors compared the energy capacity of concentric and hairpin HEXs using RT 50 as PCM. They found that the energy capacity of the hairpin HEX was 3.25 times higher than that of the concentric HEX [20]. They also conducted a numerical study on the melting and solidification processes of a U-tube HEX using three different PCMs (RT50, RT 35, and RT 27) to assess the effects of thermophysical properties and dimensionless numbers related to heat transfer [21].

In this research, the assumed heat source is derived from industrial hot water or wastewater, which contains significant amounts of waste heat typically discharged into the environment without being utilized. Waste heat recovery using heat exchangers offers an effective method for recycling thermal energy. Among various organic PCMs, paraffin wax is particularly advantageous due to its easy availability, thermal and chemical stability, cost-effectiveness, high latent heat storage capacity, and superior attributes such as flexibility in temperature application, non-corrosiveness, non-toxicity, non-flammability, and minimal supercooling [22]. Two flow configurations for double-pipe HEXs are compared numerically in this article: concentric and hairpin designs. The focus is on leveraging PCMs for LHTES and melting processes. Examining these configurations within the context of LHTES introduces a novel perspective, helping to choose the most effective design. The concentric heat exchanger (CHEX) performance is compared with other configurations reported in literature on Table 1, including vertical cylindrical systems with annular fins [23], vertical shell and tube HEX [19], triplex tube HEX via an effective dual-PCM configuration [24], multi tube HEX with Copper nanoparticles [25], triplex tube lobed HEX [26] and triplex tube through novel annular finned configurations [27], truncated-finned tanks [28,29] and tree shaped thermal energy storage [30]. However, no prior studies were identified that investigated hairpin U-tube HEXs employing three distinct PCMs. These advancements pave the way for integrating novel materials into PCM-based systems to enhance their performance and sustainability. Advancements in nanotechnology have introduced innovative materials like MgO nanoparticles (NPs) stabilized with chitosan, which exhibit remarkable properties such as high photocatalytic efficiency (89 % methylene blue dye degradation) and strong antioxidant capacities (DPPH scavenging up to 46.5 %) [7]. Similarly, materials like Zn/Ce-layered double hydroxide (Zn/Ce-LDH) exhibit exceptional adsorption capacities (up to 1297 mg/g) and rapid adsorption kinetics, with their unique properties supporting potential applications in thermal conductivity enhancement and heat transfer optimization in PCM-based systems [8].The objectives of this study are therefore to (i) examine the differences melting process in concentric and hair-pin double pipe HEX, (ii) use the commercial software Ansys-Fluent to examine how the HTF temperature and thermophysical characteristics affect the PCM melting time.

2. Computational domain

In this study, we investigate the phase change process, specifically melting and solidification, in two double pipe HEXs. The overall geometry of the equipment is illustrated in Figs. 1 and 2. Fig. 1 illustrates the configuration consisting of two concentric pipes, where the high and low-temperature fluids (HTF/LTF) circulate within the inner tube. It also presents an alternative configuration where the inner tube is U-shaped, creating a hairpin configuration within the pipe containing the PCM. The outer pipe, containing paraffin wax as the PCM, is sealed at both ends to prevent leakage, ensuring efficient LHTES. However, practical designs should include provisions for PCM's expansion. For both HEX configurations, the inner and outer diameters (ID/OD) of the outer pipe are 140 mm and 144 mm, respectively. The inner pipe dimensions are 70 mm (ID) and 72 mm (OD) for the concentric HEX and 20 mm (ID) and 24 mm (OD) for the HHEX. The total length of the inner pipe is 900 mm for the CHEX and 1600 mm for the HHEX. The thermophysical properties of

Table 1
Impact of geometry on LHTES device performance and its comparison.

PCM, Equipment	Model used in simulation	Initial Boundary Condition	Conclusions	References
RT 54 HC PCM used In triple tube lobbed HEX	Finite volume method	$T_{initial}$ =303K St = 0.317, 0.349, 0.381	Melting time reduced by 50.88 % (Ste > 0.31); 30.54 % reduction with lobes/fins, and 74.26 % with foam + nanoparticles	[26]
RT 35 and RT 82 in triplex tube HEX in novel finned configurations	Finite volume-based solver and the enthalpy-porosity formulation	$T_{initial}$=300.15K St =0.52(RT 82), 0.02 (RT 35)	Melting duration reduced by ~17 % (RT-82) and ~9 % (RT-35)	[27]
Myristic acid PCM in truncated cones	Finite element method	$T_{initial}$=333 K t_m=111 h	The STES system with PCM achieves 90.4 % efficiency, covering ~69.2 % of winter heating demand. Modular operation enhances discharge efficiency, enabling 56.30 kWh energy output from a single tank.	[29]
Paraffin wax used in conical shell double tube latent storage unit	the enthalpy-porosity formulation is used	$T_{initial}$=343K St=0.484	Melting rate enhanced by up to 42.6 % with 20 mm fins.Optimal energy storage is achieved with a 5 mm fin length at a 60° angle.	[28]
RT 50 used in double pipe heat exchanger	The enthalpy-porosity formulation	$T_{initial}$ = 358 K St=0.469	Charging time decreases with increased HTF inlet temperature; optimized flow rate required for minimum time	[33]
RT 82 PCM in the modified webbed tube heat exchanger (MWTHX)	The enthalpy-porosity formulation	T_{HTF}=366 K St =0.136	The modified webbed tube heat exchanger enhances PCM solidification by 41 %, improving thermal performance.	[35]
RT 50 PCM in the shell and-tube LHTES device.	The enthalpy-porosity formulation	$T_{initial}$=348 K St=0.315	M05 provides the highest exergy efficiency (0.77) during the melting process, making it ideal for climates with time constraints. Melting time reduced by 76 % (vertical), 66 % (horizontal), and 53 % (helical-coiled) systems	[36]
RT55 PCM in varying fin configurations	The enthalpy-porosity formulation	$T_{initial}$=343 K St=0.186	Charge time reduced by 73.7 % (variable-length fins); Discharge time reduced by 79.2 % (uniform-length fins)	[37]
Lauric acid used as PCM in fractal fins HEX	The enthalpy-porosity formulation	$T_{initial}$=293.15 K St=0.275 tm=230.4 s	68 % reduction is observed for fractal HEX compared with traditional fractal HEX	[38]
n-octadecane PCM used in PCM capsule	Enthalpy method	St=0.06,0.10,0.15	Melting rate improved by 15.29 % (central position, Ste=0.06) and 28 % (bottom position, Ste=0.15)	[39]

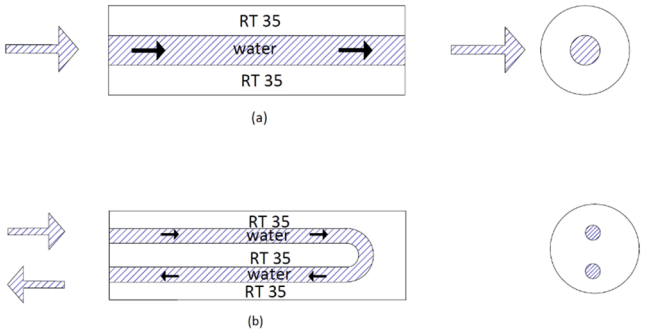


Fig. 1. Schematic diagram of the computational domain.

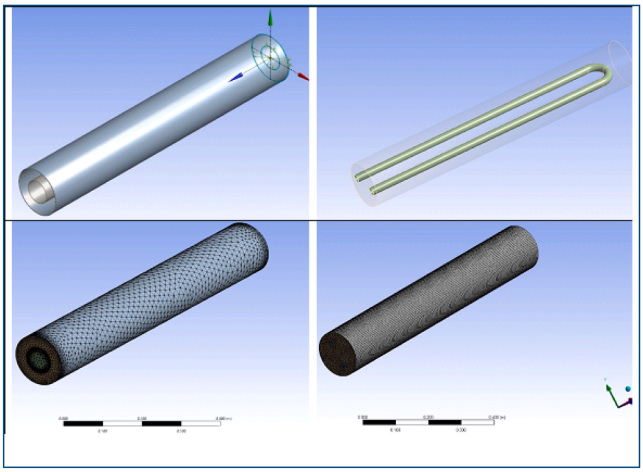


Fig. 2. Computational domain and meshing [20].

the PCM are listed in Table 2.

3. Mathematical modelling

The phase change process involves the transformation of a solid phase into a liquid phase, with distinct flow and heat transfer mechanisms in each phase. In the solid phase, heat transfer occurs primarily through conduction, whereas in the liquid phase, both conduction and convection are present. Natural convection or convection in the liquid phase arises due to density differences. The liquid phase exhibits Newtonian flow characteristics, and when solid particles are mixed with the liquid, the system functions similarly to a porous medium. The enthalpy-porosity approach effectively captures the dynamics of both phases within the mixture. The porosity of the mixture, determined by the melt fraction, varies from zero in the solid state to one in the fully liquid state. To account for the flow effects with changing porosity, the momentum balance equation is modified by adding a source term. This source term, which is proportional to velocity, uses a porosity function to progressively decrease speeds from non-zero values in the liquid state to zero as the material completely solidifies within the computational elements undergoing phase transition. By simulating flow in porous media, this technique allows the momentum equation to approximate the Kozeny-Carman equation. The porosity of the PCM changes depending on the

Table 2
Specifications of PCM (RT 35)[20].

NAME	SPECIFICATIONS
Pcm	RT 35
Solidus Temperature ***(K)***	307
Liquidus Temperature ***(K)***	309
Specific Heat Capacity ***(J/kg K)***	2000
Latent Heat ***(kJ/kg)***	160
Density ***(kg/m^3)***	820
Thermal Conductivity ***(W/m K)***	0.2
Viscosity ***(kg/m s)***	0.023
Thermal Expansion Coefficient ***(K^{-1})***	0.0006

melt fraction or liquid content, and a mushy zone constant (C_{mushy}) is incorporated into the porosity function to account for the damping effects during phase transitions. This modelling strategy has been effectively used in numerous numerical studies of phase change phenomena. In this study, the enthalpy-porosity model is employed to simulate the PCM HEX. This model uses a unified momentum balance equation to describe the movement of both liquid and solid phases. The HEX examined in this research utilizes paraffin wax as the PCM and water as the HTF. While the water remains liquid throughout the heat transfer process, the PCM transitions from solid to liquid. The benefit of the enthalpy-porosity model is its applicability to the governing equations for both the solid and liquid phases of the PCM, as well as for the water. It is expected that the HTF flow via the HEX is laminar. It is expected that the thermophysical characteristics of PCM and water will not change during the transient studies. The buoyancy effects in the PCM are modelled using the Boussinesq approximation, and the PCM is considered homogeneous and isotropic.

The following are the specifics of the governing equation [20,21]:

3.1. Governing equations

Mass conservation equation:

$$\nabla.(\rho\vec{v}) = 0 \tag{1}$$

Momentum balance equation:

$$\frac{\partial(\rho\vec{v})}{\partial t} + \nabla.(\rho\vec{v}\,\vec{v}) = -\nabla P + \nabla.(\mu\nabla\vec{v}) + \rho\vec{g}\beta(T - T_{ref}) + \vec{S} \tag{2}$$

Where,

$$\vec{S} = -A(\gamma)\vec{v} = -C_{mushy}\frac{(1-\gamma)^2}{\gamma^3 + 0.001}\vec{v} \tag{3}$$

Cmushy, commonly known as the mushy zone constant, acts as a damping coefficient that regulates the extent of velocity damping within the mushy zone. Its typical range lies between 10^4 and 10^7. In this study, the mushy zone constant has been set to 10^5 [31,32].

$$\gamma = \begin{cases} 0, & T < T_s \\ \dfrac{T - T_s}{T_l - T_s}, & T_s < T < T_l \\ 1, & T > T_l \end{cases} \tag{4}$$

Equation for Energy Balance:

$$\frac{\partial(\rho H)}{\partial t} + \nabla.(\rho\vec{v}H) = \nabla.(k\nabla T) \tag{5}$$

The definition of total enthalpy is

$$H = h + \Delta H = \left(h_{ref} + \int_{T_{ref}}^{T} C_p dT\right) + \gamma L \tag{6}$$

3.2. Initial and boundary conditions

The PCM in this study is paraffin wax, RT35. The melting (charging) processes of the PCM are examined, beginning with an initial temperature set one degree below each PCM's solidus temperature and one degree above PCM's liquidus temperature during solidification (discharging). To ensure a consistent Stefan number (St) across all experiments, the temperature of the HTF at the boundary is adjusted accordingly. The term Stefan number is defined as the ratio of sensible heat to the latent heat. In this study, the primary objective is to maximize latent heat storage using various PCMs. To achieve this, the driving force $|(T_w - T_m)|$ is managed in such a way that the sensible heat contribution remains minimal compared to latent heat. The dimensionless Stefan number plays a critical role in ensuring consistent thermal loading on the PCMs. This parameter facilitates the evaluation of thermal performance by maintaining consistent conditions for the effective utilization of latent heat in the selected PCMs. The research is conducted with Stefan numbers $St_{PCM} = \left|\frac{Cp_{PCM}\,(T_{m,\ PCM} - T_w)}{L_{PCM}}\right|$,0.35. The initial temperature for HTF and LTF are considered as 336 K and 279 K respectively. Thus, this setup is also referred to as a low-temperature heat source. In this simulation, we assume the thermophysical properties remain constant, with density variations modelled using the Boussinesq approximation. The heat transfer process is simulated using ANSYS Fluent.

4. Numerical scheme and validation

98,281 triangular cells and 1,96,311 cells for the hairpin double-pipe HEX are used to examine the phase change process in the HEX. The three-dimensional solid model and mesh are depicted in Fig. 2. The enthalpy porosity model is applied for discretization of governing equations. The SIMPLE algorithm is opted with pressure-based solver for this study. Also, to discretize momentum and energy equations, a second order upwind scheme is applied followed by PRESTO scheme for pressure correction. Ghosh et al. established grid independence for the concentric double-pipe HEX [33]. The grid independence test for the HHEX is studied using three grids where Grid 1, Grid 2 and Grid 3 refers to 603,908 cells, 655,056 cells and 924,194 cells respectively. The simulation's optimal time step is 0.1 s. As Grid 1 shows larger deviation so the simulation was run further using Grid 2 to minimize computational time for HEXs. In order to confirm the accuracy of the numerical model, the study by Gorzin et al. was reproduced in Fig. 3 employing the enthalpy-porosity model within ANSYS Fluent, followed by a comparative analysis [33,34].

5. Result and discussions

The HEX plays a vital role in recovering heat from waste fluids before they are released into the environment, enabling the repurposing of this heat to preheat process fluids. The Number of Transfer Units (NTU) method has shown that a HEX's efficiency is maximized during the phase change of one of the fluids. Furthermore, increasing the velocity of the HTF enhances the heat transfer rate. This study investigates two double-pipe HEXs of identical shell diameter and length: a hairpin double-pipe heat exchanger (HHEX) and a concentric double-pipe heat

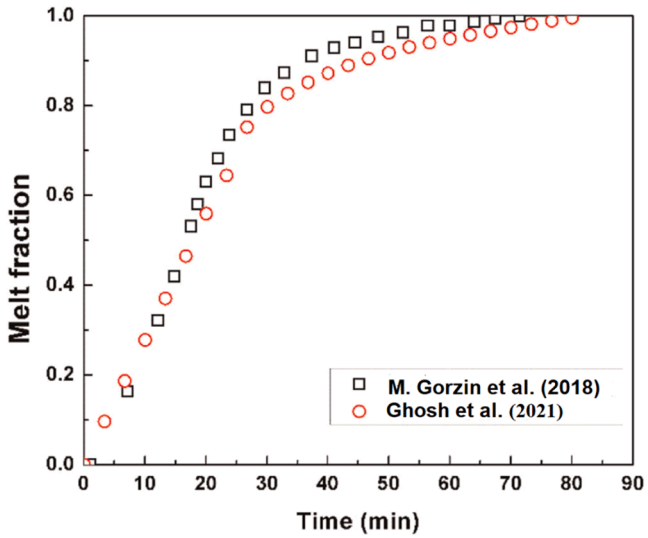


Fig. 3. Model validation [20,33,34].

exchanger (CHEX). At the starting temperature of 336 K and an HTF flow rate of 0.05 kg/s, paraffin wax (RT 35) is used in the simulation as PCM. Fig. 4 shows the melt fraction versus time distribution for complete melting and solidification process for both the HEXs. It is observed that the melting time for HHEX is approx. 146 min is lower than the CHEX which is approx. 205 min. Also, the graph shows that the time required for complete solidification is higher for HHEX (approx. 851 min) than the CHEX (approx. 227 min). Fig. 5 shows that the temperature difference between the inlet and outlet of the HTF/LTF for both the HEXs. During melting, the temperature difference for HHEX is greater than for the CHEX. This suggests that the HHEX is more efficient at extracting heat from the HTF than the CHEX, implying that altering the inlet area or U-tube diameter could enhance the overall heat storage rate. The surface area facilitating heat exchange between the PCM and HTF remains consistent for both the concentric and hairpin HEX. However, the HTF's velocity and Reynolds number rise due to the reduced inlet area, thereby accelerating the charging process. Similarly, during the solidification process, the temperature difference for LTF is higher for HHEX than CHEX indicating that the heat releases to LTF is highest. When PCM reaches the solidus temperature during the solidification process, it starts to solidify at the tube wall. Due to a density difference, the cold liquid PCM travels downward, causing the lower part of the unit's PCM to solidify at a little faster rate than the upper part. Consequently, it becomes clear that during the early stages of solidification, heat transmission is dominated by natural convection. Similar to the melting process, the solidification rate has a high beginning and a sharp decline. This is because there is a significant heat transfer temperature differential at first, but it decreases as solidification happens. Nevertheless, as time passes and the temperature differential narrows, the natural convection intensity diminishes. This is due to the fact that heat conduction dominates the solidification process in its later phases. At this point, the solidification layer gets thicker and thicker, and the heat resistance increases, causing the solidification rate to decline until it hits zero. Fig. 7 shows the contours of melt fraction for both HEXs. The ratio of the liquid fraction to time is mathematically represented by the melting rate. Four distinct phases can be identified in the melting process by examining the evolution of the melting front. Because viscous forces predominate in the early phase, the melting front advances outward parallel to the HTF tube wall. During this phase, the melting rate first begins at the maximal value and then rapidly decreases. It makes sense that the temperature difference is greatest at first and subsequently decreases as melting occurs. Here, from Figure, the liquid PCM is visible at around 3 min but slightly delayed in case of CHEX. It means that liquid PCM is observed where melting process is controlled by natural convection. Because of

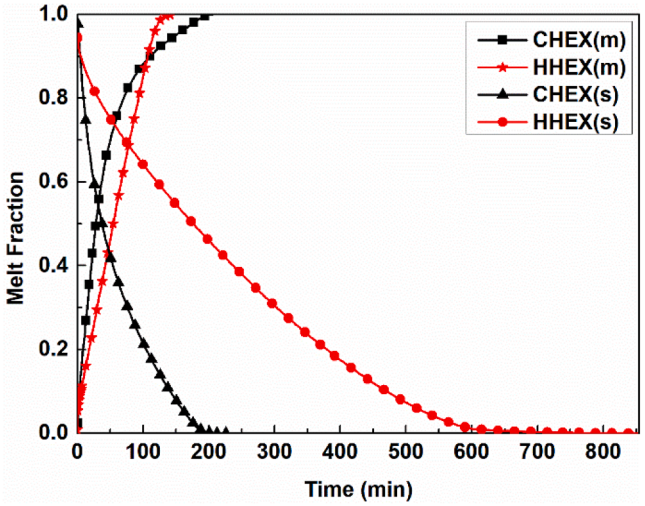


Fig. 4. Influence of melt fraction during charging and discharging.

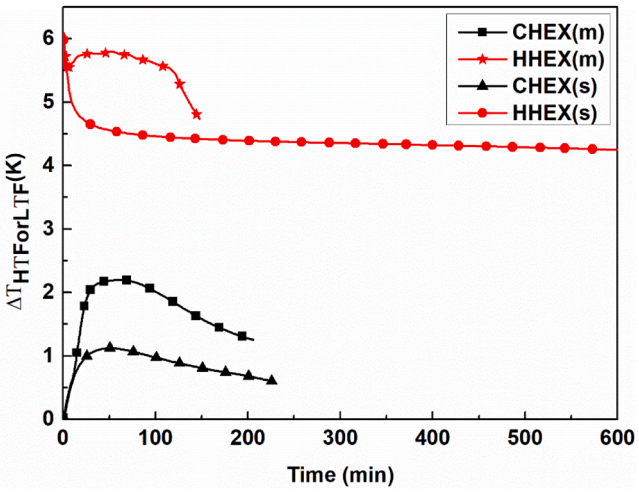


Fig. 5. Influence of inlet-outlet temperature difference.

the decreased input velocity and Reynolds number in the case of CHEX, the liquid PCM is noticed slightly later, and the conduction mechanism dominates heat transmission. After 25 min, the solid and liquid phase can be easily identified. As it absorbs latent heat, the solid PCM starts to melt and liquefy close to the HTF tube. Initially, the liquid layer remains stable near the wall as viscous forces dominate over buoyant and inertial forces. The liquid layer gows as melting progresses, enabling buoyancy forces to overcome viscous forces. Natural convection currents are generated due to the density difference between the liquid and solid PCM. These currents, driven by buoyancy forces, accelerate the melting process from the inlet to the outlet, causing to thermal stratification. Since the density of solid phase of PCM is greater than its liquid phase. The volume of PCM decreases with a drop in the temperature as paraffin wax is transformed from liquid to solid phase. Additionally, conduction dominates in the lower region, whereas the higher convective zone contrasts along the axis and expands radially. The liquid PCM gathers near the top of this vertical configuration because to gravity, which speeds up melting in the direction of the outlet section. Clearly, we can say that rate of melting is higher in case of HHEX and after 25 min the natural convection is dominating for both the cases. Due to the formation of dead zone located at the bottom right of the HHEX (85 min), the process slows down as the distance between the inner pipe and PCM increases. In this zone, conduction dominates as there is no natural convection visible and thermal conductivity drops which makes the process slow. The energy stored in the CHEX is 2061 kJ, while in the HHEX it is 2096 kJ, indicating nearly identical energy storage. However, the time required to store this energy in the HHEX is 146 min, significantly less than the 207 min required for the CHEX. Figure shows the heat flux variation of RT 35 (St=0.35) with respect to time for both melting and solidification processes. From the graph, we observe there is sudden decrease in heat flux with time. The heat flux decreases over time in both processes. Initially, there is a substantial rate of change in heat flux, which gradually diminishes as the melting or solidification progresses. Notably, following the formation of a melt fraction, the heat flux approaches a near-minimum level, and the rate of change in heat flux significantly slows, as illustrated in Fig. 6. During the charging process, the heat flux ranges from 0.30 kW/m^2 to 0.007 kW/m^2 for the HHEX and from 0.4 kW/m^2 to 0.006 kW/m^2 for the CHEX. During the solidification process, the heat flux ranges from 0.31 kW/m^2 to 0.0006 kW/m^2 for the HHEX and from 0.39 kW/m^2 to 0.01 kW/m^2 for the CHEX. This indicates that at the start of the process, the contact time between the PCM and HTF is at its maximum, while the heat transfer rate is relatively low. In contrast, for the HHEX, the contact time is notably low due to the high velocity of the HTF. Conversely, in the CHEX, the extended contact duration between the HTF and the PCM

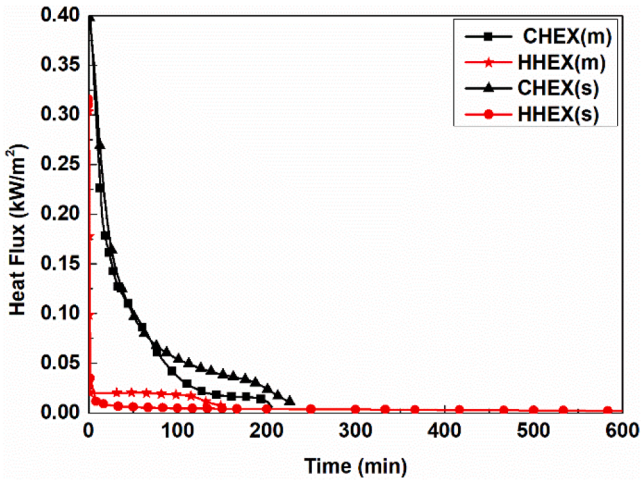


Fig. 6. Influence of Heat Flux during charging and discharging.

facilitates more efficient heat transfer. This prolonged interaction allows the PCM to absorb heat from the HTF over a more extended timeframe. Consequently, the velocity of the HTF decreases in the CHEX, leading to an increase in the melting rate. In the HHEX, the length of the pipe is nearly double that of the concentric double-pipe HEX due to the use of a U-shaped tube. This configuration results in higher HTF velocities, thereby enhancing the charging process and allowing the same heat source to store more energy in less time.

Further, the average energy calculation has been done for both the HEXs which is shown in Fig. 8. Here, the energy stored is calculated as, the energy stored in the system is determined as the product of the latent heat and the mass of the phase change material (PCM).The energy storage rate is defined as the energy stored per unit time .From Fig. 1, it is known that the outer surface of the pipe size is similar but the amount of PCM content in HHEX is 1.25 times higher than that of concentric. Therefore, the energy stored will be higher in case of hairpin. The melting time is also higher for CHEX case (Fig. 4) for the same St, 0.35. The quantity of heat stored per unit of time is known as the average energy storage capacity. After calculating, the energy storage is 196 W and 108 W for hairpin and concentric HEX respectively. Finally, from changing the design from concentric to hairpin, the energy storage increases by 1.8 times using RT 35 paraffin wax.

6. Conclusion

The study includes the comparison of two different types of HEXs i.e., concentric and hairpin using RT 35 for both the cases. The inlet temperature and flow rate were taken as 336 K and 0.05 kg/sec respectively for all the cases.

1. A larger energy storage capacity is achieved by switching the heat exchanger from a concentric to a hair-pin type of PCM mass, increasing it from 8.3 kg to 10.7 kg. The evaluated increase in energy storage capacity for hairpin and concentric heat exchangers are 196 W and 108 W respectively.

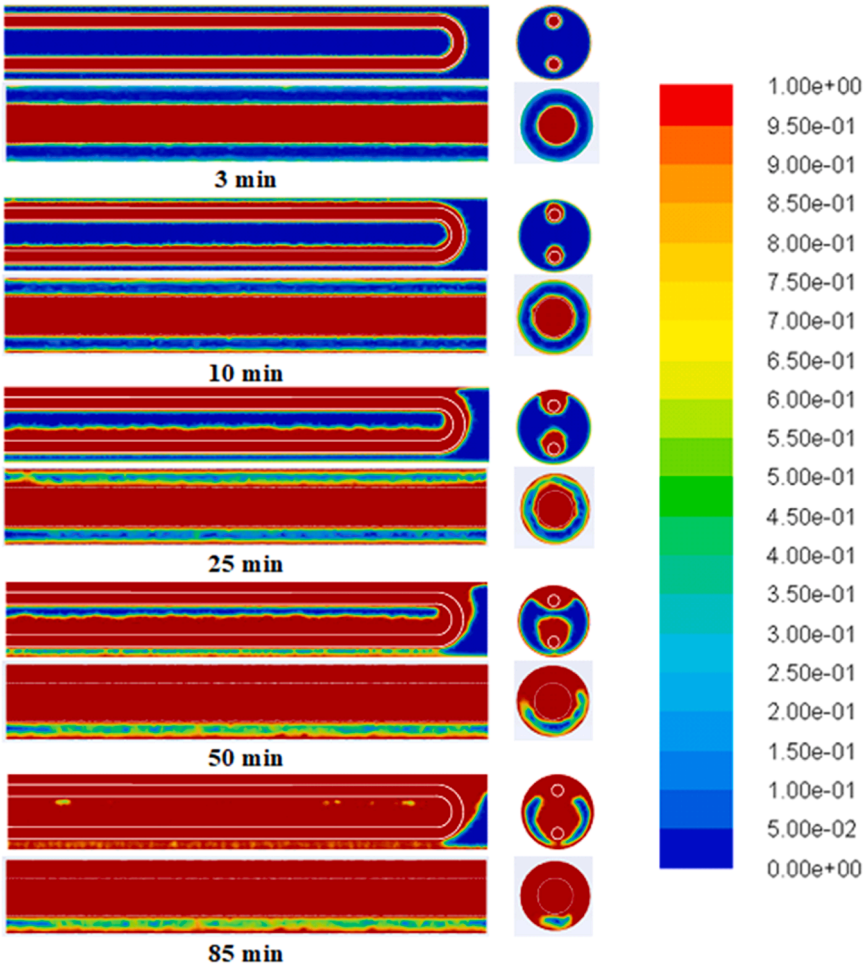


Fig. 7. Contour of melt-fraction concentric and hair-pin double pipe HEX (St = 0.35).

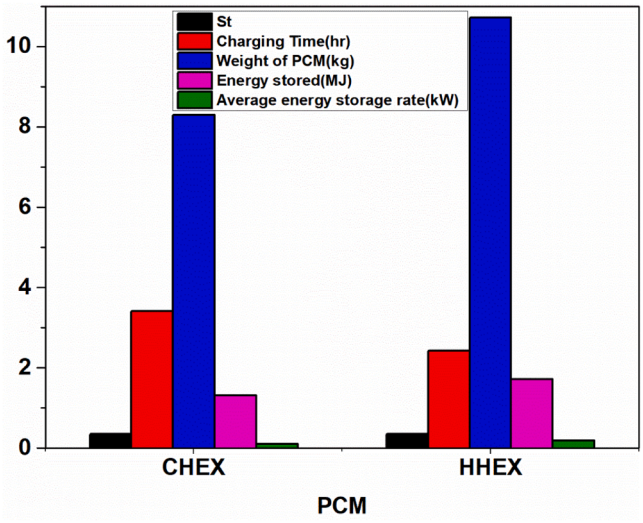


Fig. 8. Analysis of energy storage.

2. The redesign from a concentric to a hairpin double-pipe heat exchanger (HEX) resulted in an increased rate of energy storage due to the higher velocity of the HTF.
3. Due to the curved surface area or heat transfer area between HTF and PCM is same for concentric and hairpin HEX. Simultaneously, the velocity and Reynolds number increases due to lower inlet area of hairpin due to which the melting rate becomes faster. Also, the velocity of HTF for hairpin and concentric HEX is 0.16 m/sec and 0.01 m/sec respectively.

Different HTF flow rates and heat exchanger orientations or inclinations can be used to perform comparable simulations. Additionally, the experimental validation must enhance the LHTES design. These research will assist in choosing the best design of heat exchanger with PCM. An efficient latent heat energy storage device may be achieved by optimizing the energy storage rate and the energy stored.

Funding

The Science & Engineering Research Board (SERB) of India provided financial support (file no. SPG/2021/004530), for which the authors are thankful.

CRediT authorship contribution statement

Pallavi Kumari: Writing – original draft. **Vinamr Saksena:** Formal analysis. **Rishabh Jha:** Resources. **Debasree Ghosh:** Writing – review & editing.

Declaration of competing interest

The authors declare that none of their known financial conflicts or interpersonal connections could have influenced the work that was published in this paper.

Data availability

Data will be made available on request.

References

[1] B.K. Choure, T. Alam, R. Kumar, A review on heat transfer enhancement techniques for PCM based thermal energy storage system, J. Energy Storage 72 (2023), https://doi.org/10.1016/j.est.2023.108161.
[2] J.L. Holechek, H.M.E. Geli, M.N. Sawalhah, R. Valdez, A global assessment: can renewable energy replace fossil fuels by 2050? Sustainability. 14 (8) (2022) https://doi.org/10.3390/su14084792.
[3] L. Kumar, M. Hasanuzzaman, N.A. Rahim, Global advancement of solar thermal energy technologies for industrial process heat and its future prospects: a review, Energy Convers. Manage 195 (2019) 885–908, https://doi.org/10.1016/j.enconman.2019.05.081.
[4] D. Ürge-Vorsatz, L.F. Cabeza, S. Serrano, C. Barreneche, K. Petrichenko, Heating and cooling energy trends and drivers in buildings, Renew. Sustain. Energy Rev. 41 (2015) 85–98, https://doi.org/10.1016/j.rser.2014.08.039.
[5] M. Isaac, D.P. van Vuuren, Modeling global residential sector energy demand for heating and air conditioning in the context of climate change, Energy Policy 37 (2) (2009) 507–521, https://doi.org/10.1016/j.enpol.2008.09.051.
[6] S. Seddegh, X. Wang, A.D. Henderson, Z. Xing, Solar domestic hot water systems using latent heat energy storage medium: a review, Renew. Sustain. Energy Rev. 49 (2015) 517–533, https://doi.org/10.1016/j.rser.2015.04.147.
[7] I. Ben Amor, et al., Enhancing oxidant and dye scavenging through MgO-based chitosan nanoparticles for potential antioxidant coatings and efficient photocatalysts, Biomass Convers. Biorefinery 14 (24) (2024) 32343–32357, https://doi.org/10.1007/s13399-023-04923-1.
[8] A.M. Ramezani, F. Amiri Panah, M. Heydari Dokoohaki, E. Adnan Azooz, R. Ahmadi, S. Nazari, Zn/Ce-layered double hydroxide for adsorptive removal of doxycycline from water, Mater. Chem. Phys. 318 (2024) 129223, https://doi.org/10.1016/j.matchemphys.2024.129223.
[9] M.J. Hosseini, A.A. Ranjbar, K. Sedighi, M. Rahimi, A combined experimental and computational study on the melting behavior of a medium temperature phase change storage material inside shell and tube heat exchanger, Int. Commun. Heat Mass Transf. 39 (9) (2012) 1416–1424, https://doi.org/10.1016/j.icheatmasstransfer.2012.07.028.
[10] M.J. Hosseini, M. Rahimi, R. Bahrampoury, Experimental and computational evolution of a shell and tube heat exchanger as a PCM thermal storage system, Int. Commun. Heat Mass Transf. 50 (2014) 128–136, https://doi.org/10.1016/j.icheatmasstransfer.2013.11.008.
[11] M. Esapour, M.J. Hosseini, A.A. Ranjbar, Y. Pahamli, R. Bahrampoury, Phase change in multi-tube heat exchangers, Renew. Energy 85 (2016) 1017–1025, https://doi.org/10.1016/j.renene.2015.07.063.
[12] K.A.R. Ismail, F.A.M. Lino, R.C.R. da Silva, A.B. de Jesus, L.C. Paixão, Experimentally validated two dimensional numerical model for the solidification of PCM along a horizontal long tube, Int. J. Therm. Sci. 75 (2014) 184–193, https://doi.org/10.1016/j.ijthermalsci.2013.08.008.
[13] P. Talebizadehsardari, J.M. Mahdi, H.I. Mohammed, M.A. Moghimi, A. Hossein Eisapour, M. Ghalambaz, Consecutive charging and discharging of a PCM-based plate heat exchanger with zigzag configuration, Appl. Therm. Eng. 193 (2021) 116970, https://doi.org/10.1016/j.applthermaleng.2021.116970.
[14] M.A. Said, et al., Accelerated charging dynamics in shell-and-multi-tube latent heat storage systems for building applications, J. Energy Storage 81 (2024) 110286, https://doi.org/10.1016/j.est.2023.110286.
[15] M. Fadaei, M. Izadi, E. Assareh, A. Ershadi, Conjugated non-Newtonian phase change process in a shell and tube heat exchanger: a parametric-geometric analysis, Appl. Therm. Eng. 220 (2023) 119795, https://doi.org/10.1016/j.applthermaleng.2022.119795.
[16] F. Agyenim, P. Eames, M. Smyth, Heat transfer enhancement in medium temperature thermal energy storage system using a multitube heat transfer array, Renew. Energy 35 (1) (2010) 198–207, https://doi.org/10.1016/j.renene.2009.03.010.
[17] H.-O. Sayehvand, S. Abolfathi, B. Keshavarzian, Investigating heat transfer enhancement for PCM melting in a novel multi-tube heat exchanger with external fins, J. Energy Storage 72 (2023) 108702, https://doi.org/10.1016/j.est.2023.108702.
[18] S. Kalaiselvam, M. Veerappan, A.Arul Aaron, S. Iniyan, Experimental and analytical investigation of solidification and melting characteristics of PCMs inside cylindrical encapsulation, Int. J. Therm. Sci. 47 (7) (2008) 858–874, https://doi.org/10.1016/j.ijthermalsci.2007.07.003.
[19] C. Nie, J. Liu, S. Deng, Effect of geometric parameter and nanoparticles on PCM melting in a vertical shell-tube system, Appl. Therm. Eng. 184 (2021) 116290, https://doi.org/10.1016/j.applthermaleng.2020.116290.
[20] P. Kumari, D. Ghosh, A comparative numerical analysis of concentric and hairpin heat exchanger for efficient energy storage using phase-change material, J. Therm. Anal. Calorim. 148 (21) (2023) 12211–12224, https://doi.org/10.1007/s10973-023-12501-w.
[21] P. Kumari, A. Raj, D. Ghosh, Selection of phase change material for latent heat thermal energy storage using a hair-pin heat exchanger: numerical study, J. Therm. Sci. Eng. Appl. (2024) 1–33, https://doi.org/10.1115/1.4065490.
[22] K. Chopra, et al., Thermal and chemical reliability of paraffin wax and its impact on thermal performance and economic analysis of solar water heater, Energy Sustain. Dev. 73 (2023) 39–53, https://doi.org/10.1016/j.esd.2023.01.004.
[23] Y. Zhu, Y. Yu, Y. Qiu, Effect of fins with unequal length on the performance of cylindrical latent heat storage system, J. Energy Storage 35 (2021) 102224, https://doi.org/10.1016/j.est.2020.102224.
[24] M. Mozafari, A. Lee, S. Cheng, A novel dual-PCM configuration to improve simultaneous energy storage and recovery in triplex-tube heat exchanger, Int. J. Heat. Mass Transf. 186 (2022) 122420, https://doi.org/10.1016/j.ijheatmasstransfer.2021.122420.
[25] M. Gorzin, M.J. Hosseini, M. Rahimi, R. Bahrampoury, Nano-enhancement of phase change material in a shell and multi-PCM-tube heat exchanger, J. Energy Storage 22 (2019) 88–97, https://doi.org/10.1016/j.est.2018.12.023.

[26] A. NematpourKeshteli, M. Iasiello, G. Langella, N. Bianco, Optimization of the thermal performance of a lobed triplex-tube solar thermal storage system equipped with a phase change material, Heliyon. 10 (16) (2024) e36105, https://doi.org/10.1016/j.heliyon.2024.e36105.
[27] J. Khan, K. Nithyanandam, and P. Singh, "Computational study on transient thermal performance enhancement of phase change materials in triplex tube heat exchanger through novel annular-finned configurations," *Numer. Heat Transf. Part A Appl.*, pp. 1–18, doi: 10.1080/10407782.2024.2380813.
[28] M.A. Alnakeeb, M. Shatarah, M.K. Hamza, M.A.A. Salam, H.M. Teamah, The effect of fin geometry on the thermal performance of a conical shell double tube latent storage unit, J. Energy Storage 94 (2024) 112471, https://doi.org/10.1016/j.est.2024.112471.
[29] N. Bianco, A. Fragnito, M. Iasiello, G.M. Mauro, Multiscale analysis of a seasonal latent thermal energy storage with solar collectors for a single-family building, Therm. Sci. Eng. Prog. 50 (2024) 102538, https://doi.org/10.1016/j.tsep.2024.102538.
[30] N. Bianco, A. Fragnito, M. Iasiello, G.M. Mauro, Solid-solid PCM-based tree-shaped thermal energy storage system for solar cooling application, Sol. Energy 283 (2024) 113040, https://doi.org/10.1016/j.solener.2024.113040.
[31] M.R. Kadivar, M.A. Moghimi, P. Sapin, C.N. Markides, Annulus eccentricity optimisation of a phase-change material (PCM) horizontal double-pipe thermal energy store, J. Energy Storage 26 (2019) 101030, https://doi.org/10.1016/j.est.2019.101030.
[32] D. Ghosh, C. Guha, Numerical simulation of paraffin wax melting in a rectangular cavity using CFD, Indian Chem. Eng. 62 (3) (2020) 314–328, https://doi.org/10.1080/00194506.2019.1689183.
[33] D. Ghosh, P. Kumar, S. Sharma, C. Guha, J. Ghose, Numerical investigation on latent heat thermal energy storage in a phase change material using a heat exchanger, Heat Transf 50 (5) (2021) 4289–4308, https://doi.org/10.1002/htj.22075.
[34] M. Gorzin, M.J. Hosseini, A.A. Ranjbar, R. Bahrampoury, Investigation of PCM charging for the energy saving of domestic hot water system, Appl. Therm. Eng. 137 (2018) 659–668, https://doi.org/10.1016/j.applthermaleng.2018.04.016.
[35] A.H.N. Al-Mudhafar, A.F. Nowakowski, F.C.G.A. Nicolleau, Performance enhancement of PCM latent heat thermal energy storage system utilizing a modified webbed tube heat exchanger, Energy Reports 6 (2020) 76–85, https://doi.org/10.1016/j.egyr.2020.02.030.
[36] J. Wołoszyn, K. Szopa, G. Czerwiński, Enhanced heat transfer in a PCM shell-and-tube thermal energy storage system, Appl. Therm. Eng. 196 (2021) 117332, https://doi.org/10.1016/j.applthermaleng.2021.117332.
[37] S. Tiari, A. Hockins, M. Mahdavi, Numerical study of a latent heat thermal energy storage system enhanced by varying fin configurations, Case Stud. Therm. Eng. 25 (2021) 100999, https://doi.org/10.1016/j.csite.2021.100999.
[38] X. Luo, et al., Numerical study on enhanced melting heat transfer of PCM by the combined fractal fins, J. Energy Storage 45 (2022) 103780, https://doi.org/10.1016/j.est.2021.103780.
[39] T. Bouzennada, F. Mechighel, A. Filali, K. Ghachem, L. Kolsi, Numerical investigation of heat transfer and melting process in a PCM capsule: effects of inner tube position and stefan number, Case Stud. Therm. Eng. 27 (2021) 101306, https://doi.org/10.1016/j.csite.2021.101306.